Journal of Catalysis **184,** 479–490 (1999)
Article ID jcat.1999.2469, available online at http://www.idealibrary.com on IDEAL®

Catalytic Performance and Catalyst Structure of Nickel–Magnesia Catalysts for CO_2 Reforming of Methane

Yang-Guang Chen, Keiichi Tomishige,[1] Kota Yokoyama, and Kaoru Fujimoto[2]

Department of Applied Chemistry, School of Engineering, The University of Tokyo, Hongo, Bunkyo-ku, Tokyo 113-8656, Japan

Received November 11, 1998; revised March 1, 1999; accepted March 2, 1999

The catalytic performance of nickel–magnesia catalysts in CO_2 reforming of methane and the factors influencing carbon deposition during the reaction were investigated by a comparative study of reduced $Ni_xMg_{1-x}O$ solid solution and magnesia-supported Ni metal (Ni/MgO) catalysts. Reduced $Ni_xMg_{1-x}O$ solid solution catalysts generally showed higher resistance to carbon formation than Ni/MgO. From the combination of catalytic properties with the characterization results of XRD, TEM, FTIR, and dispersion measurements, it was found that the excellent anticoking performance of reduced solid solution catalyst with low Ni content is attributable to high dispersion of reduced Ni species, basicity of support surface, and nickel-support interaction. © 1999 Academic Press

Key Words: **CO_2 reforming of methane; anticoking performance; nickel–magnesia catalysts; nickel–support interaction.**

INTRODUCTION

Considerable attention has been paid to the catalytic reforming of CH_4 with CO_2 to synthesis gas ($CH_4 + CO_2 \rightarrow 2CO + 2H_2$) in recent years (1–10). This reaction has very important environmental implications since both CH_4 and CO_2 contribute to the greenhouse effect. They are also two of the most abundant carbon-containing materials. Therefore, converting these two gases into a valuable synthesis gas may not only reduce atmospheric emissions of CO_2 and CH_4 but also satisfy the requirement of many synthesis processes in the chemical industry. In addition, since the synthesis gas produced by this reaction has a high CO content, it is more suitable for the synthesis of valuable oxygenated chemicals than that produced by conventional steam reforming.

Great efforts have been focused on the development of catalysts which show high activity and stability. It is recognized that most of the group VIII metals are more or less effective for CH_4/CO_2 reaction in terms of CH_4 conversion and selectivity to synthesis gas (4, 11–19). However, there are some factors of deactivation. They are generally solid reaction of the active metal with the support, carbon deposition, and the sintering of active metals. Among them, carbon deposition is the most serious problem and appears unavoidable, especially for nickel-based catalysts. Gadalla and Sommer have established the conditions for carbon-free operation using thermodynamic calculations (1). To prevent carbon formation, a high CO_2/CH_4 ratio and a high reaction temperature are required, but the temperature must be lower than an upper-temperature limit where nickel carbide forms. It is also known that catalysts based on noble metals are less sensitive to coking than nickel catalysts, probably due to the lower solubility of carbon in noble metals (4, 7, 11, 15, 18). But the high cost and limited availability of noble metals restrict their applications. It has been reported that sulfur passivation of nickel catalysts can suppress carbon deposition effectively, and based on this finding, SPARG (sulfur-passivated reforming) is already running on a larger scale (18). However, in this case, catalytic activity is sacrificed to a large extent, although the rate of carbon formation decreases more than the reforming rate. The effect of the nature of the support has also been noted in recent years. Osaki *et al*. have determined the composition of the intermediate hydrocarbon species using pulse surface reaction rate analysis (20). They found that the number of hydrogen atoms involved in the surface CH_x species had a correlation with the anticoking performance of these Ni catalysts. Zhang *et al*. have investigated Ni/La_2O_3 catalysts. These catalysts had high stability under diluted $CH_4 + CO_2$, but a small decline of activity with time on stream was observed on the catalyst under undiluted $CH_4 + CO_2$ feed (21–23). Another catalyst system noteworthy for its excellent anticoking performance is nickel-containing spinel or solid solution. Chen and Ren have convincingly shown that carbon deposition can be markedly suppressed when $NiAl_2O_4$ is formed during the pretreatment procedure (24). It was found that a $Ni_{0.03}Mg_{0.97}O$ solid solution catalyst, which was reduced with H_2 at 1123 K, can realize carbon-free operation at 1123 K over 3000 h in the reforming of CH_4 with CO_2 and studies related to this catalyst have been carried out (25–35). Furthermore, this catalyst was found to have high

[1] To whom correspondence should be addressed at Department of Applied Chemistry, School of Engineering, The University of Tokyo, 7-3-1, Hongo, Bunkyo-ku, Tokyo 113-8656, Japan. Fax: +81-5689-0469. E-mail: tomi@hongo.ecc.u-tokyo.ac.jp.

[2] To whom correspondence should be addressed.

0021-9517/99 $30.00
Copyright © 1999 by Academic Press
All rights of reproduction in any form reserved.

resistance to carbon formation in CO_2 reforming and steam reforming of methane under low $H_2O/CH_4 = 1/1$ conditions (27). It has been reported that reduced NiO/MgO with 9.2–28.6 wt% NiO has shown excellent stability for 120 h, while reduced NiO/CaO, NiO/SrO, and NiO/BaO exhibited lower activity and stability. Furthermore, the catalytic properties of NiO/MgO have been investigated (36–40).

In this paper we investigated the relation between catalyst structure and catalytic properties, especially activity and carbon deposition behavior, on NiO–MgO solid solution ($Ni_xMg_{1-x}O$) and supported (Ni/MgO) catalysts. It is expected that these catalysts will have different Ni particle sizes and different strengths of interaction between active nickel species and support surfaces. The effect of catalyst structure on catalytic activity and coke formation is discussed in this paper.

EXPERIMENTAL

Catalyst Preparation

$Ni_xMg_{1-x}O$ solid solution catalysts were prepared by coprecipitating nickel acetate (>98.0%, Kanto) and magnesium nitrate (>99.2%, Kanto) aqueous solutions with potassium carbonate (>99.5%, Kanto). The details of catalyst preparation are described in previous papers (27, 30). After being filtered and washed with hot water, the precipitate was dried at 393 K overnight and then calcined at 1223 K for 10 h. The Ni content ranged from $x = Ni/(Ni + Mg) = 0.03$ to 0.15. We used these catalysts after H_2 reduction at 1123 K before the reaction. Therefore, in the strict sense, the structure of the working catalyst was not a solid solution. But in this paper, $Ni_xMg_{1-x}O$ after reduction and during the catalytic reaction is also denoted as $Ni_xMg_{1-x}O$ solid solution catalyst. MgO-supported Ni metal catalysts (Ni/MgO) were prepared by impregnating homemade MgO with the acetone solution of nickel acetylacetonate complex (>99%, Soekawa Chemicals), followed by drying at 393 K overnight. The preparation method of MgO support was the same as that for $Ni_xMg_{1-x}O$. Ni loading of supported catalysts ranged from the atomic ratio of $Ni/(Ni + Mg) = 0.3$ to 3%. Ni/MgO catalysts were not calcined at high temperatures in order to make smaller amounts of solid solution. Before use, all these catalysts were pressed into tablets and crushed to 20- to 40-mesh particles.

Activity Test

Activity measurements were carried out in a fixed-bed continuous-flow reactor made of a 6-mm-i.d. quartz tube. Catalyst weight was about 0.05 g. After the catalysts were reduced in flowing H_2 (99.9995%, Takachiho) at 1123 K for 0.5 h, a reactant gas feed consisting of a mixture of CH_4 (99.99%, Takachiho) and CO_2 (99.99%, Takachiho) was introduced into the reactor under 0.1 MPa and W/F = 0.1–1.2 g h/mol. The reaction temperature varied from 773 to 973 K. The effluent gas was analyzed with an on-line TCD gas chromatograph using 2 m of active carbon as the separating column. An ice bath was set between the reactor exit and the GC sampling valve in order to remove water from the effluent gas.

Catalyst Characterization

Catalyst surface area was measured by the BET method and nitrogen sorption at 77 K with Gemini (Micromeritics). Bulk phase analysis of catalysts was performed on an RINT 2400 (Rigaku) X-ray diffractometer with Cu$K\alpha$ radiation.

The consumption measurements of H_2 and O_2 were carried out in a static volumetric glass high-vacuum system. Research grade gases (H_2, 99.9995%; O_2, 99.99%, Takachiho) were used without further purification. Before consumption of H_2 and O_2, the prereduced catalysts were treated in H_2 at 1123 K for 0.5 h, followed by evacuation. The amount of consumption was measured at room temperature for H_2 and at 873 K for O_2. The pressure of the gas phase at the equilibrium state was about 26.3 kPa in each case.

The morphology of the catalysts was observed by means of a JEM-2010F microscope operated at 200 kV. After reduction with H_2 or catalytic reaction at 773 K, the samples were stored under vacuum until the measurements were made. Samples were dispersed in tetrachloromethane by supersonic waves and put on Cu grids for the TEM observation under atmosphere.

FTIR measurements for the adsorption of CO and CO_2 on various catalysts at room temperature were carried out in an *in situ* IR cell combined with a closed circulating system. About 0.15 g of catalyst was pressed into 20 mm ϕ thin self-supporting wafers for the use of IR measurements. IR spectra were recorded by MAGNA-IR 550 (Nicolet) using the transmission method and a MCT detector with 2 cm^{-1} resolution. After the catalysts were reduced at 1123 K for 0.5 h and after subsequent evacuation, the sample temperature was cooled to room temperature. FTIR spectra of CO and CO_2 adsorption were obtained after the introduction and evacuation of CO (99.95%, Takachiho) and CO_2 (99.99%, Takachiho) at some pressure.

The accumulation of carbonaceous species on the catalyst surface during the reforming of CH_4 with CO_2 as a function of time on stream (2, 30, and 60 min, respectively) and their reactivity toward hydrogenation were characterized by the temperature-programmed hydrogenation (TPH) method. The catalyst (0.05 g) was reduced in H_2 flow at 1123 K for 0.5 h prior to the introduction of the reactant gas ($CH_4/CO_2 = 1/1$, W/F = 0.1 g h/mol, 773 K). After the reduced catalyst was exposed to the reaction conditions for 2, 30, or 60 min, the feed gas was switched to Ar for 10 min, and then the reactor was quickly cooled to room temperature,

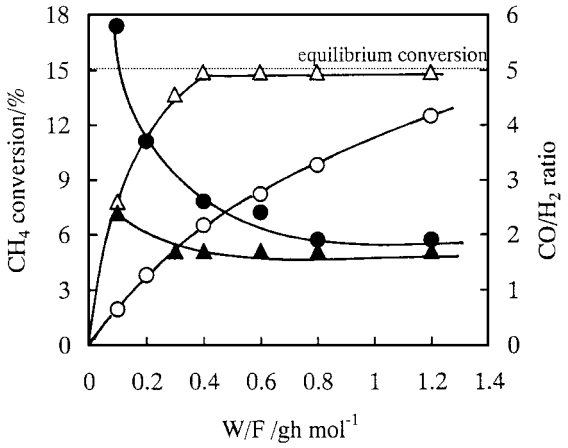

FIG. 1. The influence of contact time on the catalytic activity (○, △) and CO/H_2 ratio of the product gas (●, ▲) in CO_2 reforming of methane over $Ni_{0.03}Mg_{0.97}O$ solid solution (○, ●) and 3 mol% Ni/MgO (△, ▲) catalysts at 773 K. Reaction conditions: $CH_4/CO_2 = 1/1$, 0.1 MPa; catalyst weight, 0.05 g.

followed by TPH characterization. In TPH experiments, pure H_2 (99.9995%, Takachiho) was used. The catalyst temperature was raised from room temperature to 1123 K at a heating rate of 20 K/min. CH_4 and CO_2 were detected, and a small amount of CO_2 was desorbed below 773 K. This may be due to the decomposition of the product which is formed by the reaction between CO_2 and catalyst or CO_2 adsorbed on stronger basic sites. The signal of CH_4 was recorded continuously by FID equipped with no separating column. No products than other methane were observed in the analysis of the frequent sampling gas by another GC with the separating column and FID. Two peaks of methane formation were observed in TPH profiles. One appeared between 550 and 700 K and is designated as α-carbon; the other appeared above 873 K and is named β-carbon. In our previous paper (29), it was found that β-carbon was mainly due to the hydrogenation of adsorbed CO_2 on support and β-carbon was responsible for carbon deposition. Therefore, in this paper, only the data on β-carbon are discussed.

RESULTS AND DISCUSSION

Comparison between Solid Solution and Supported Catalysts in Catalytic Performance

The influence of contact time on catalytic activity in the reforming of CH_4 with CO_2 over $Ni_{0.03}Mg_{0.97}O$ solid solution and 3 mol% Ni/MgO catalysts at 773 K is shown in Fig. 1. A 3 mol% Ni/MgO was more active in the CH_4–CO_2 reaction than $Ni_{0.03}Mg_{0.97}O$. The equilibrium conversion was achieved at 3 mol% Ni/MgO at $W/F \geq 0.4$ g h/mol, while W/F higher than 1.2 g h/mol was required for $Ni_{0.03}Mg_{0.97}O$ to approach the equilibrium level. The CO/H_2 ratio in the product gas was always higher than unity, which is the stoichiometry of this reaction. This was due to the reverse water-gas shift reaction ($H_2 + CO_2 \rightarrow H_2O + CO$) (41, 42). At $W/F = 0.1$ g h/mol, both catalysts showed conversions far from the equilibrium level; therefore we chose this reaction condition in the comparison of the catalytic activity. Equilibrium conversion is also shown in Fig. 1. Under this reaction condition, equilibrium methane conversion can be calculated to be about 15% (32). Experimental methane conversion at the reaction equilibrium was a little lower than that by thermodynamic calculation. This may be due to error in product analysis and temperature measurement.

Figure 2 shows the CO formation rate as a function of time on stream over $Ni_{0.03}Mg_{0.97}O$ solid solution and 3 mol% Ni/MgO catalysts at various reaction temperatures. On the basis of thermodynamic calculations, the CO formation rate at the reaction equilibrium corresponds to about 2200, 1300, and 500 μmol/g s at 973, 873, and 773 K. Under the reaction condition of Fig. 2, methane conversion on these two catalysts was far from the equilibrium level. With increasing reaction temperatures, the catalytic activities increase significantly. The apparent activation energies are

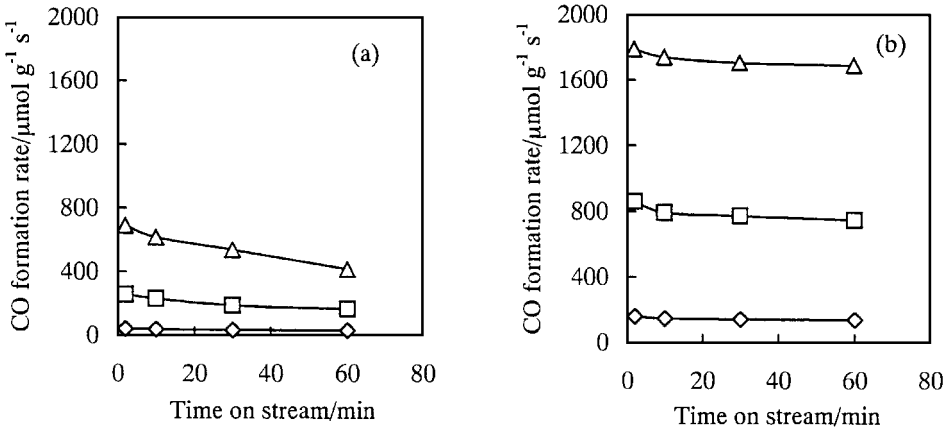

FIG. 2. CO formation rate in CO_2 reforming of methane as a function of time on stream over $Ni_{0.03}Mg_{0.97}O$ solid solution (a) and 3 mol% Ni/MgO (b) catalysts at 773 K (◇), 873 K (□), and 973 K (△). Reaction conditions: $CH_4/CO_2 = 1/1$, 0.1 MPa, $W/F = 0.1$ g h/mol; catalyst weight, 0.05 g.

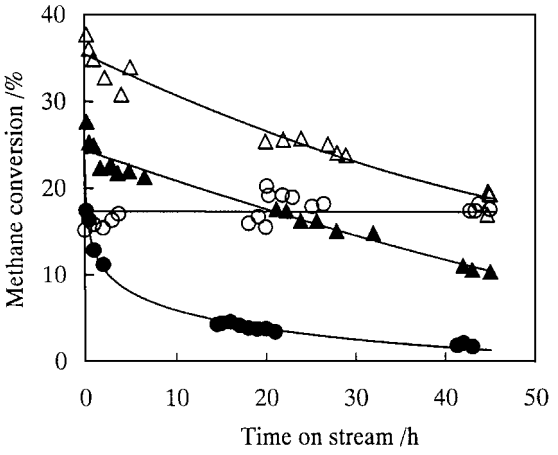

FIG. 3. Effects of H_2 addition to $CH_4 + CO_2$ on the activity and stability of $Ni_{0.03}Mg_{0.97}O$ solid solution (●, ○) and 3 mol% Ni/MgO (▲, △) catalysts. CH_4/CO_2 (●, ▲), $CH_4/CO_2/H_2$ (○, △). Reaction conditions: $CH_4/CO_2/N_2 = 50/25/25$, $CH_4/CO_2/H_2/N_2 = 50/25/5/20$, 0.1 MPa, W/F = 0.5 g h/mol for $Ni_{0.03}Mg_{0.97}O$ and 0.2 g h/mol for 3 mol% Ni/MgO; reaction temperature, 1023 K; catalyst weight, 0.05 g.

18 kcal/mol for $Ni_{0.03}Mg_{0.97}O$ and 21 kcal/mol for 3 mol% Ni/MgO, respectively. For $Ni_{0.03}Mg_{0.97}O$, the catalyst deactivation was observed at each temperature, and it was more significant at higher reaction temperatures. In our previous paper, it was proven that the deactivation of $Ni_{0.03}Mg_{0.97}O$ catalysts cannot be ascribed to the carbon deposition, since when the activity reached zero, the amount of carbon on the catalyst was almost zero (28). From the observation that the color of the catalyst was gray before reaction and green after reaction, it is suggested that the deactivation of $Ni_{0.03}Mg_{0.97}O$ may be caused by the oxidation of reduced Ni by CO_2 and H_2O during the reaction. A considerable amount of carbon was deposited on 3 mol% Ni/MgO during the reaction, as shown later. But significant deactivation was not observed. This implies that a large part of the carbon does not poison the active site, and its morphology seems to be filamentous (24, 43–45). However, it has been reported that the accumulation of filamentous carbon will finally result in an increased pressure drop of the reactor and a physical breakdown of the catalyst (44).

Furthermore, we examined the catalyst stability at 1023 K under $CH_4/CO_2/N_2 = 50/25/25$ and $CH_4/CO_2/H_2/N_2 = 50/25/5/20$. It can be seen from Fig. 3 that a $Ni_{0.03}Mg_{0.97}O$ solid solution catalyst lost most of its activity after 43 h on a $CH_4/CO_2/N_2$ stream, the relative activity decreasing from 1 to 0.09. Especially, the initial deactivation was significant. In contrast, the relative activity decreased from 1 to 0.37 for a 3 mol% Ni/MgO catalyst under the same conditions. On the other hand, when 5% H_2 was introduced into the reactant gas feed, the deactivation on $Ni_{0.03}Mg_{0.97}O$ disappeared completely. This result indicated that the addition of H_2 inhibited the deactivation by the oxidation of reduced Ni on $Ni_{0.03}Mg_{0.97}O$. Although hydrogen also exists in the products, the effect of hydrogen addition was significant. This suggested that the catalyst oxidation proceeds at the inlet of the catalyst bed because the partial pressure of hydrogen is very low, especially in the experiment without the addition of H_2. But the deactivation of 3 mol% Ni/MgO was still observed under the H_2-added condition, and the relative activity after a 43-h reaction increased to 0.51. Figure 4 shows the XRD patterns of these two catalysts after reduction and after 43 h on a $CH_4/CO_2/H_2/N_2$ stream at 1023 K. No peaks of carbon were detectable on a $Ni_{0.03}Mg_{0.97}O$ solid solution catalyst. But the peak at $2\theta = 26.5^\circ$, which can be assigned to graphite was observed on 3 mol% Ni/MgO. On

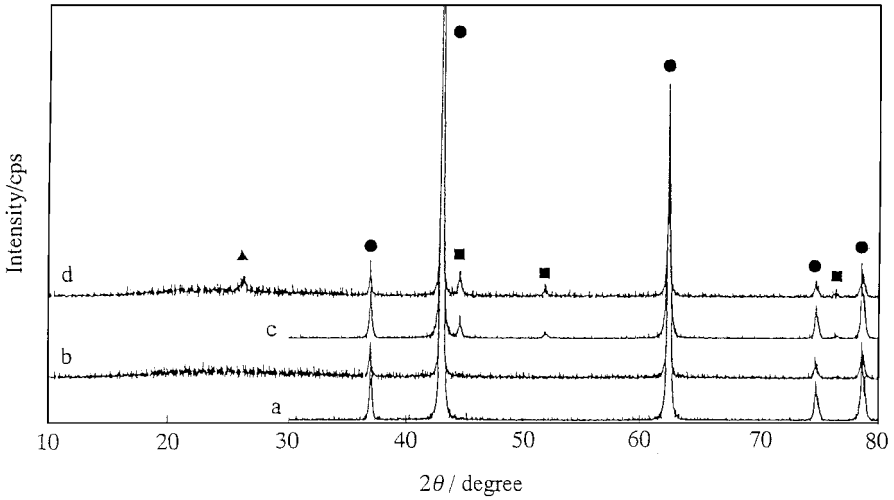

FIG. 4. XRD patterns for $Ni_{0.03}Mg_{0.97}O$ solid solution (a, b) and 3.0 mol% Ni/MgO (c, d) catalysts after H_2 reduction at 1123 K for 0.5 h (a, c) and after reaction under $CH_4/CO_2/H_2/N_2$ at 1023 K for 43 h. Reaction conditions: $CH_4/CO_2/H_2/N_2 = 50/25/5/20$, 0.1 MPa, W/F = 0.5 g h/mol for $Ni_{0.03}Mg_{0.97}O$ and 0.2 g h/mol for 3 mol% Ni/MgO, 1023 K; catalyst weight, 0.05 g. Assignment: (●) Ni-Mg-O solid solution or MgO, (■) Ni metal, (▲) graphite.

the other hand, it is noted that the intensity of the peaks at $2\theta = 44.5$, 51.8, and 76.4° on 3 mol% Ni/MgO after reaction was apparently enhanced compared with that in the reduced catalyst. This indicates that the sintering of Ni metal particles probably occurred during the reaction, which may also cause the deactivation of 3 mol% Ni/MgO. However, it seems that aggregation of Ni metal particles was not observed on $Ni_{0.03}Mg_{0.97}O$, which is suggested by the fact that no change is observed in the XRD pattern between the reduced catalyst and that after the reaction. In the case of 3 mol% Ni/MgO, the aggregation of nickel and the formation of carbon may cause the deactivation.

Figure 5 shows profiles of temperature-programmed hydrogenation of the sample after CH_4–CO_2 reaction. The amount of β-carbon is listed in Table 1. The peak due to β-carbon could not be distinguished above 700 K on $Ni_{0.03}Mg_{0.97}O$ solid solution catalysts (Fig. 5a). A slight shift of baseline observed in the TPH profile apparently caused about 30–40 μmol-C g^{-1} of β-carbon on $Ni_{0.03}Mg_{0.97}O$ solid solution catalysts after 2-, 30-, and 60-min reactions, but the amount was not increased with reaction time on $Ni_{0.03}Mg_{0.97}O$ solid solution catalysts. In contrast, a clear peak due to β-carbon was observed on three other catalysts and the peak intensities increased proportionally with the reaction time. These data were obtained at $W/F = 0.1$ g h/mol, where methane conversion on $Ni_{0.03}Mg_{0.97}O$ solid solution catalysts was far from the equilibrium. At $W/F =$ 1.2 g h/mol, where methane was close to the equilibrium as shown in Fig. 1, carbon deposition was not observed on the catalyst. On $Ni_{0.10}Mg_{0.90}O$ solid solution catalysts, deposited carbon was observed as shown in Fig. 5b. This indicated that nickel magnesia solid solution catalysts with a high Ni content did not exhibite as high a resistance to carbon deposition as $Ni_{0.03}Mg_{0.97}O$ solid solution catalysts. In addition, as shown in Fig. 5c, the peak of β-carbon was also observed on $Ni_{0.03}Mg_{0.97}O$ calcined at 773 K, which was prepared by calcining the precipiate at 773 K for 10 h after drying. High-temperature calcination and solid solution formation during catalyst preparation seem to be necessary for the inhibition of carbon deposition. On 3 mol%

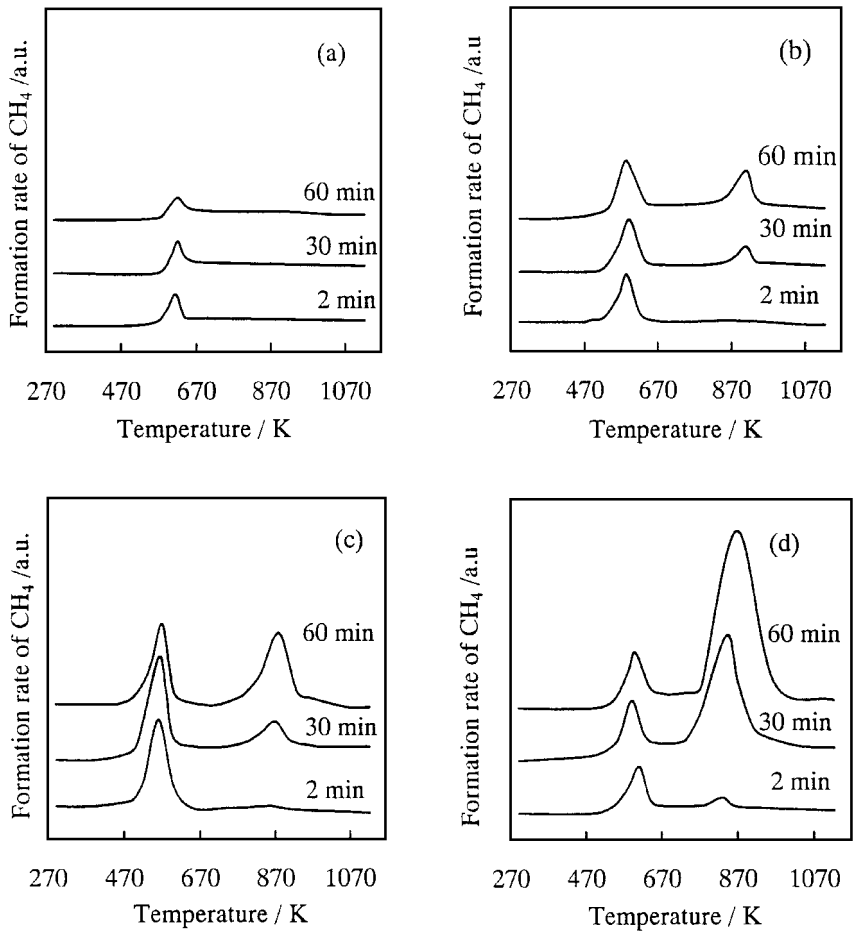

FIG. 5. Profiles of temperature-programmed hydrogenation on the samples after the reaction for 2, 30, and 60 min. (a) $Ni_{0.03}Mg_{0.97}O$ solid solution, (b) $Ni_{0.10}Mg_{0.90}O$ solid solution, (c) $Ni_{0.03}Mg_{0.97}O$ calcined at 773 K, (d) 3 mol% Ni/MgO. Reaction conditions: $CH_4/CO_2 = 1/1$, 0.1 MPa, $W/F =$ 0.1 g h/mol; catalyst weight, 0.05 g; reaction temperature, 773 K. The calcination temperature of (a) and (b) was 1223 K.

TABLE 1

Properties of Nickel–Magnesia Solid Solution and Magnesia-Supported Nickel Catalysts for CO_2 Reforming of Methane

Catalyst	Preparation method	Ni/(Ni + Mg) (%)	T_c[a] (K)	BET ($m^2\ g^{-1}$)	H_2[b] (μmol g^{-1})	O_2[c] (μmol g^{-1})	D_{red}[d] (%)	D_{disp}[e] (%)	Deposited carbon: Amount[f] (μmol-C g^{-1})	Deposited carbon: TOF[g] ($10^{-3}\ s^{-1}$)	CH_4 Conv.[h] (%)	CO formation: Rate[i] (μmol g^{-1} s^{-1})	CO formation: TOF[j] (s^{-1})	Carbon selectivity[k] (10^{-2}%)
$Ni_{0.03}Mg_{0.97}O$	Coprecipitation	3	1223	19	3.1	10.5	2.9	30	0	0.0	2	40	6.5	0.0
$Ni_{0.03}Mg_{0.97}O$	Coprecipitation	3	973	42	12.4	146.7	40.4	9	111	1.3	8	158	6.4	2.0
$Ni_{0.03}Mg_{0.97}O$	Coprecipitation	3	773	53	18.6	212.2	58.5	9	182	1.4	11	240	6.5	2.2
$Ni_{0.05}Mg_{0.95}O$	Coprecipitation	5	1223	29	4.2	55.5	9.3	8	84	2.9	5	97	11.5	2.5
$Ni_{0.10}Mg_{0.90}O$	Coprecipitation	10	1223	30	14.9	130.4	11.4	11	129	1.2	8	155	5.2	2.3
$Ni_{0.15}Mg_{0.85}O$	Coprecipitation	15	1223	29	4.8	39.0	2.5	12	85	2.6	6	123	12.8	2.0
0.3 mol% Ni/MgO	Impregnation	0.3	—	18	2.4	21.8	58.6	11	62	3.7	5	87	18.1	2.0
1.0 mol% Ni/MgO	Impregnation	1	—	18	4.1	84.9	69.0	5	185	6.5	6	127	15.5	4.3
3.0 mol% Ni/MgO	Impregnation	3	—	16	3.9	226.5	62.4	2	485	17.8	8	138	17.7	10.1

[a] Calcination temperature.
[b] H_2 consumption at 298 K.
[c] O_2 consumption at 873 K.
[d] Reduction degree: $2x$(O_2 consumption)/(total Ni), assuming that $Ni^0 + 1/2O_2 \rightarrow NiO$.
[e] Dispersion of reduced Ni particles: amount ratio of H_2 consumption to O_2 consumption, assuming $H/Ni_s = 1$ and total reduced Ni = $2x$(O_2 consumption).
[f] The difference of β-carbon amount: (β-carbon after reaction for 60 min)-(β-carbon after reaction for 2 min), the amount of β-carbon deposited on each catalysts was estimated by the TPH method. Reaction conditions were as follows: 773 K, 0.1 MPa, $CH_4/CO_2 = 1/1$, W/F = 0.1 g h/mol, 60 min, 0.05 g-cat.
[g] TOF was estimated on the basis of H_2 consumption assuming $H/Ni_s = 1$.
[h] CH_4 conversion under the reaction conditions: 773 K, 0.1 MPa, $CH_4/CO_2 = 1/1$, W/F = 0.1 g h/mol, 60 min, 0.05 g-cat.
[i] CO formation rate under reaction conditions: 773 K, 0.1 MPa, $CH_4/CO_2 = 1/1$, W/F = 0.1 g h/mol, 60 min, 0.05 g-cat.
[j] TOF was calculated on the basis of H_2 consumption results.
[k] Carbon selectivity: (TOF of carbon formation)/(TOF of carbon formation + CO formation).

Ni/MgO, a large amount of deposited carbon was observed in Fig. 5d.

Characterization of Catalyst

The results of the characterization of the catalysts are summarized in Table 1. It is thought that the amount of O_2 consumption at 873 K corresponds to the total amount of reduced Ni in the catalysts on the basis of $Ni^0 + 1/2O_2 \rightarrow NiO$. The amount of H_2 consumption at room temperature is thought to give the number of surface Ni atoms on the basis of $H/Ni_s^0 = 1$. From Table 1, it can be seen that there is a large difference in the degree of reduction (the ratio of reduced Ni to total Ni). Ni/MgO catalysts exhibited high reducibility, their reduction degree was around 60%, and the reducibility did not seem to be influenced by Ni loading. This indicates that the majority of Ni^{2+} in reduced Ni/MgO catalysts is in the metallic state. Unreduced Ni may form solid solution catalysts. In contrast, the degree of reduction of Ni was below 10% on solid solution catalysts. These were increased with the nickel content in solid solutions, consistent with the report about the reducibility of NiO–MgO solid solutions (46). In addition, $Ni_{0.03}Mg_{0.97}O$ calcined at 773 and 973 K showed a higher BET surface area and a higher reduction degree than calcined at 1223 K. This is probably because the crystal size was smaller and a solid solution was not formed completely at lower temperatures. If the H_2 and O_2 consumption in Table 1 be corresponds to the number of surface Ni atoms and the number of reduced Ni atoms, respectively, the dispersion of nickel metal particles is estimated by the ratio of H_2 consumption to O_2 consumption as shown in Table 1.

XRD patterns of catalysts after reduction in H_2 flow at 1123 K for 30 min are shown in Fig. 6. The diffraction peaks at 36.9, 42.9, 62.3, and 78.6° can be ascribed to a nickel magnesia solid solution or MgO. Table 2 shows the diffraction

TABLE 2

Diffraction Angle of Nickel–Magnesia Solid Solution Catalysts

Catalyst	Diffraction angle 2θ[a]/°
$Ni_{0.03}Mg_{0.97}O$	42.93
$Ni_{0.05}Mg_{0.95}O$	42.93
$Ni_{0.10}Mg_{0.90}O$	42.96
$Ni_{0.15}Mg_{0.85}O$	42.98
3 mol% Ni/MgO	42.90, 43.02

[a] Cu$K\alpha$.

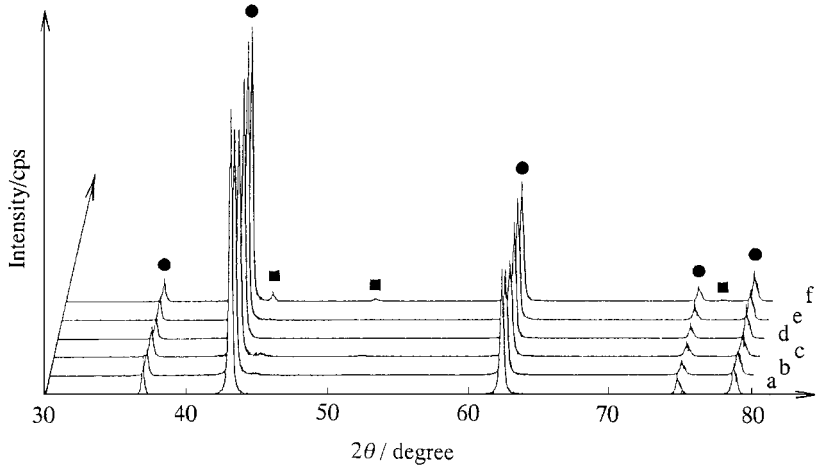

FIG. 6. XRD patterns of the solid solution and supported catalysts after H_2 reduction. (a) $Ni_{0.03}Mg_{0.97}O$ solid solution, (b) $Ni_{0.05}Mg_{0.95}O$ solid solution, (c) $Ni_{0.10}Mg_{0.90}O$, (d) 0.3 mol% Ni/MgO, (e) 1.0 mol% Ni/MgO, (f) 3.0 mol% Ni/MgO. Assignment: (●) Ni-Mg-O solid solution or MgO, (■) Ni metal.

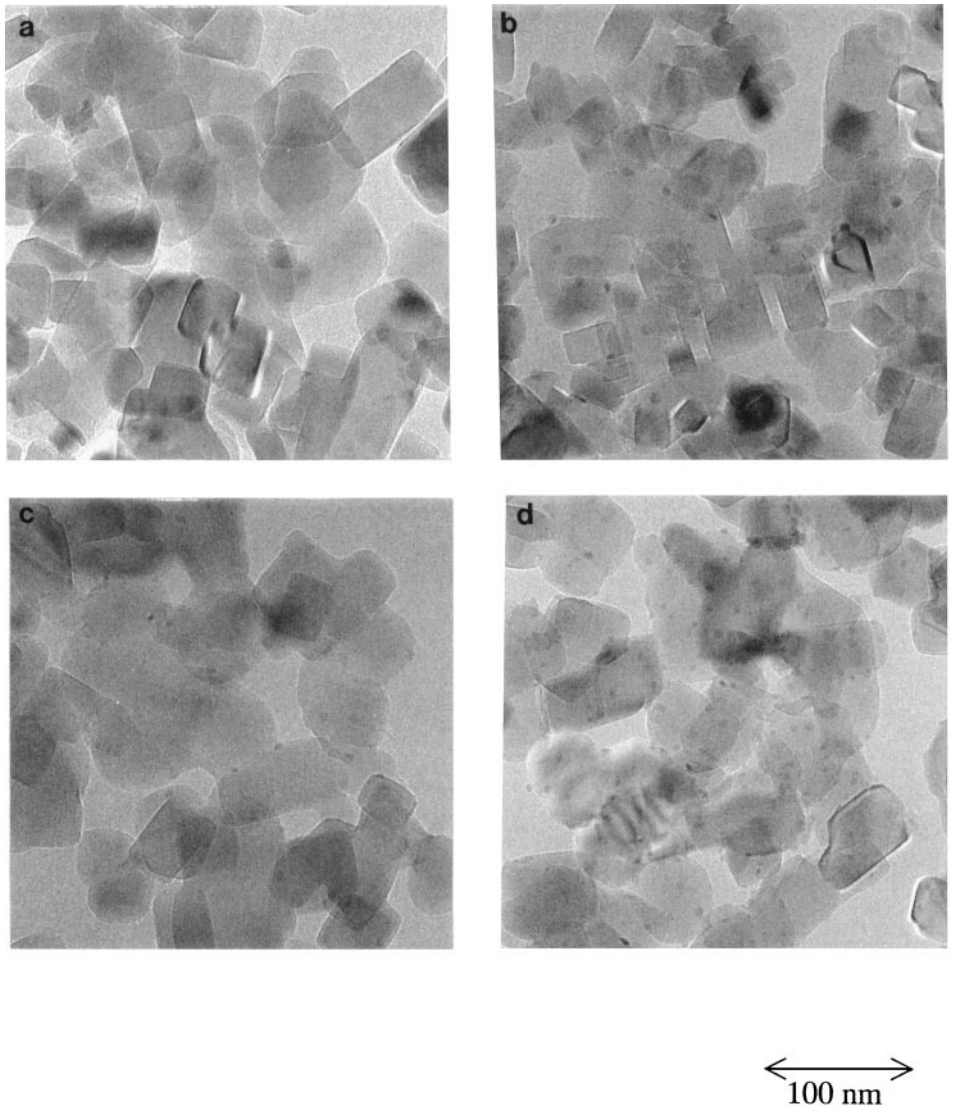

FIG. 7. TEM images of catalysts after H_2 reduction at 1123 K. (a) $Ni_{0.03}Mg_{0.97}O$, (b) $Ni_{0.10}Mg_{0.90}O$, (c) 0.3 mol% Ni/MgO, (d) 3.0 mol% Ni/MgO.

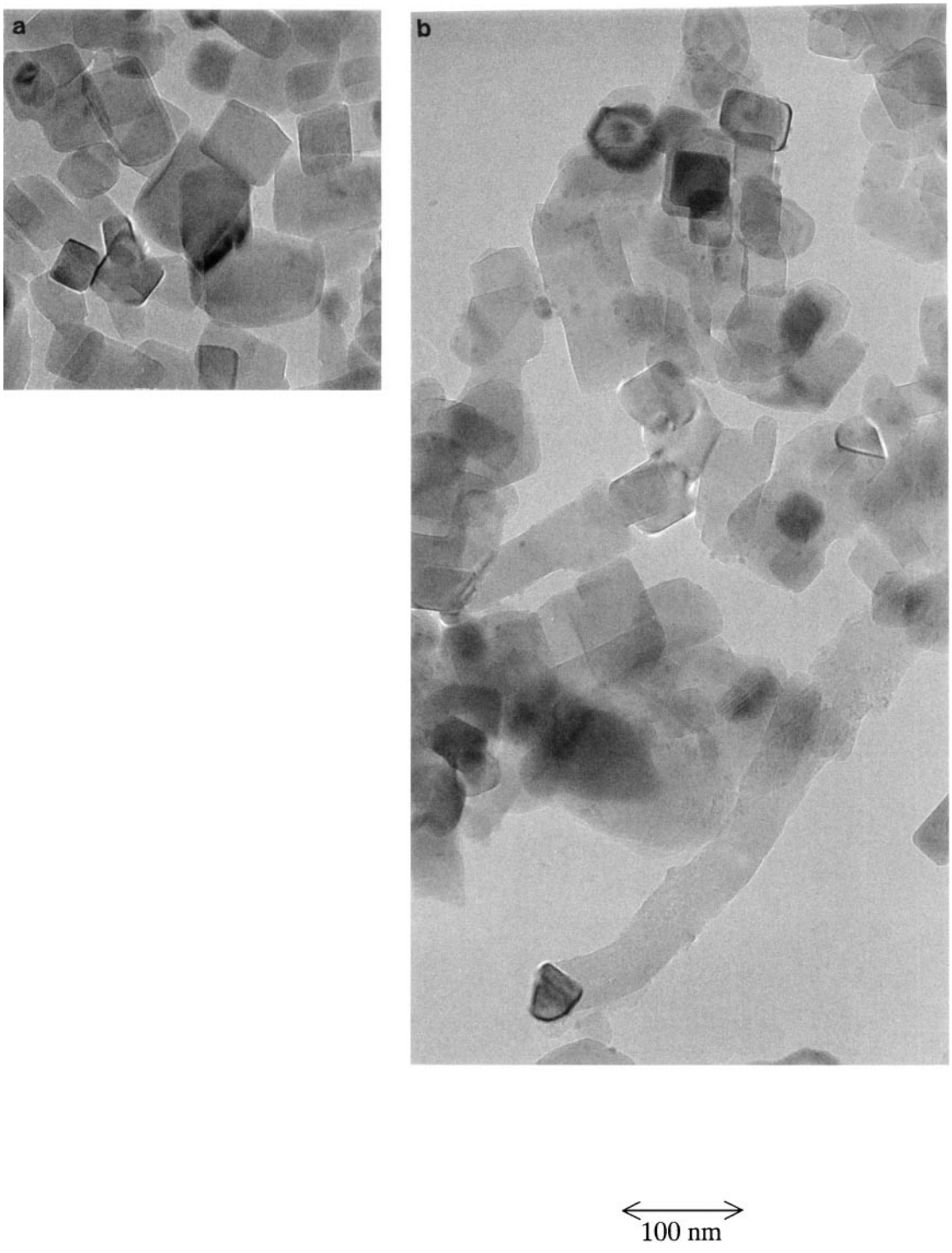

FIG. 8. TEM images of catalysts after CO_2 reforming of CH_4. (a) $Ni_{0.03}Mg_{0.97}O$, (b) 3 mol% Ni/MgO. Reaction conditions: $CH_4/CO_2 = 1/1$, W/F = 0.1 g h/mol, total pressure 0.1 MPa, 773 K, 1 h.

angle of the maximum peak. The small shift in the diffraction angle is due to the effect of Ni^{2+} ions incorporated in NiO–MgO solid solutions as reported (47). The diffraction peaks at 44.5, 51.8, and 76.4° can be attributed to metallic Ni. On 3 mol% Ni/MgO, the sharp peaks due to Ni metal were observed. This indicated that 3 mol% Ni/MgO had very large nickel particles. This corresponded to very low H_2/O_2 in Table 1. In addition, a strong peak at 42.90°

with a shoulder peak at 43.02° was observed on 3 mol% Ni/MgO. The strong peak can be assigned to MgO. The shoulder peak can be assigned to a NiO–MgO solid solution with $Ni/(Ni + Mg) = 0.3$, which is estimated on the basis of Ref. (47). This indicated that 3 mol% Ni/MgO contained three phases: nickel metal, MgO, and solid solution with high nickel content. This agrees with the result that the reduction degree did not reach 100% as listed in Table 1. Since no calcination was performed during the pretreatment of Ni/MgO catalysts, a major part of Ni^{2+} would be reduced before its diffusion into MgO lattices to form solid solutions. Unlike Ni/MgO catalysts, $Ni_xMg_{1-x}O$ solid solution catalysts experienced high temperature calcination, and Ni^{2+} ions were diffused into MgO bulk to form solid solutions.

TEM images of catalysts reduced at 1123 K are shown in Fig. 7. Only a few Ni particles (about 3–4 nm) are observed on the plane of cubic support (unreduced solid solution) for $Ni_{0.03}Mg_{0.97}O$, and nickel particles were not observed on most support cubes as shown in Fig. 7a. This is in agreement with the high dispersion and low reduction degree. In Fig. 7b, we observed that many more Ni particles with diameters mainly ranging between 4 and 8 nm appeared on $Ni_{0.10}Mg_{0.90}O$ catalysts. Obviously, the increase of Ni content resulted in the aggregation of metal particles. The 0.3 mol% Ni/MgO had Ni particles with size distribution from 3 to 10 nm (Fig. 7c). The 3.0 mol% Ni/MgO has a considerably broader particle size distribution relative to the others (Fig. 7d). We can calculate the average particle size according to the equation $d_s = \sum n_i d_i^3 / \sum n_i d_i^2$ on the basis of counting the diameter of numerous particles. The average particle sizes of $Ni_{0.03}Mg_{0.97}O$, $Ni_{0.10}Mg_{0.90}O$, 0.3 mol% Ni/MgO, and 3.0 mol% Ni/MgO were 3.9, 6.3, 5.0, and 6.4 nm, respectively. From these results, the dispersion can be calculated to be 0.25, 0.15, 0.19, and 0.15 on the basis of (49). There is a large difference between these values and the H_2/O_2 ratios in Table 1, especially on 3 mol% Ni/MgO. Judging from the XRD results, this dispersion of 3 mol% Ni/MgO from TEM must be too high. The size of the image field of TEM may be so limited that very large Ni particles failed to be observed. In addition, many more nickel particles seem to be present on $Ni_{0.03}Mg_{0.97}O$ than those observed by TEM. This was discussed in the previous paper (30).

Figure 8 shows the TEM images of $Ni_{0.03}Mg_{0.97}O$ and 3.0 mol% Ni/MgO catalysts after the reforming reaction at 773 K for 1 h. The image of $Ni_{0.03}Mg_{0.97}O$ catalysts did not change before and after reaction, indicating that no carbon was formed on this catalyst surface during the reaction. This agrees with TPH results. However, the TEM image of 3.0 mol% Ni/MgO shows the presence of tubular filamentous carbon with large Ni particle at the end. The diameter of this whisker carbon is very close to the Ni crystal size and the Ni crystal is pear shaped as reported by Baker *et al.* (48). It is worth moting that whisker carbon was formed only on the particles with diameters larger than 30 nm as shown in Fig. 8b. The carbon deposition was not observed on smaller nickel particles. This means that the formation of a carbon whisker is disfavored on small Ni particles even on 3.0 mol% Ni/MgO catalysts.

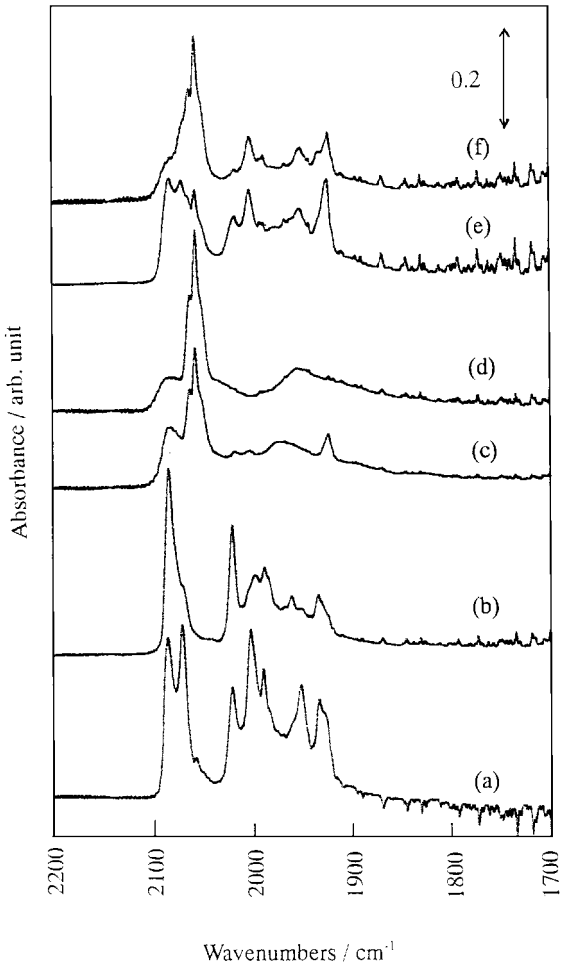

FIG. 9. FTIR spectra of CO adsorption on catalysts. (a) $Ni_{0.03}Mg_{0.97}O$, (b) $Ni_{0.05}Mg_{0.95}O$, (c) $Ni_{0.07}Mg_{0.93}O$, (d) $Ni_{0.10}Mg_{0.90}O$, (e) 1.0 mol% Ni/MgO, (f) 3.0 mol% Ni/MgO. Reduction pretreatment, H_2 reduction at 1123 K; FTIR measurement, room temperature, $P_{CO} = 13.3$ kPa, 2 cm^{-1} resolution.

Figure 9 shows FTIR spectra of CO adsorption on the catalysts after H_2 reduction. The assignment of the IR peaks, listed in Table 3, was from previous literature (49, 50). On $Ni_{0.03}Mg_{0.97}O$ and $Ni_{0.05}Mg_{0.95}O$, a few kinds of nickel carbonyl species that interacted with the support surface were observed. But physisorbed $Ni(CO)_4$ and linear and bridge CO were observed on nickel magnesia solid solution catalysts with nickel content higher than 0.07. In contrast, on 1.0 and 3.0 mol% Ni/MgO catalysts, a few kinds of nickel carbonyl species, which interacted with the support surface as well as with linear and bridge CO and $Ni(CO)_4$, were observed. The result that so many kinds of CO species

TABLE 3

Assignment of FTIR of CO Adsorption on Nickel–Magnesia Solid Solution and Supported Catalysts

Wavenumber/cm^{-1}	Species
2083, 2020, 1985	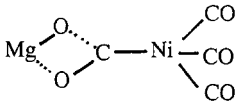
2070, 2002, 1950	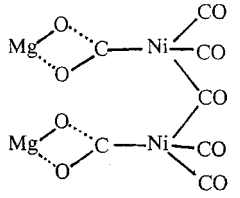
2057	$Ni(CO)_4$
2100–2030	Linear CO on Ni metal surface
2000–1900	Bridge CO on Ni metal surface

were observed on supported catalyst seems to correspond to the wide distribution of nickel particle size. On the other hand, it seems that solid solution catalysts with high nickel content are homogeneous. These trends are consistent with TEM results.

Figure 10 shows FTIR spectra of CO_2 adsorption on catalysts after H_2 reduction. The assignment of adsorbed CO_2 was from previous reports (51–55). Two kinds of bidentate carbonate (1670/1305 and 1625/1272 cm^{-1}) and a kind of bicarbonate (1652/1405 cm^{-1}) were observed. CO_2 adsorbed on solid solutions with low Ni content was very similar to that on MgO, on which bidentate carbonate was mainly observed. But on solid solutions with higher Ni contents, bicarbonate was increased and bidentate carbonate was decreased. The adsorbed species of CO_2 seems to be determined by the surface composition of nickel and magnesium ions. On the other hand, FTIR spectra of CO_2 adsorbed on 1.0 and 3.0 mol% Ni/MgO catalysts were not similar to those of MgO but to those of NiO–MgO solid solutions with high Ni content. This indicated that the support surface changed from MgO to the solid solution on supported catalysts. This is supported by the result that the solid solution phase with high Ni content was found by XRD analysis. It is found that the solid solution is formed on supported catalysts at near-surface.

Structural images of solid solution catalysts with low and high nickel contents, supported catalysts, which are suggested from the catalyst characterization results, are depicted in Fig. 11. Solid solution catalysts with low Ni content have nickel particles with high dispersion and MgO-like support surfaces (Fig. 11a). Solid solution catalysts with high nickel contents have nickel particles with low dispersion and the support surface is similar to a solid solution (Fig. 11b). Ni/MgO-supported catalysts have nickel particles with wide size distributions, and the support surface is similar to a solid solution with high nickel content (Fig. 11c).

Correlation between Catalyst Structure and Catalytic Performance in CO_2 Reforming of CH_4

Figure 12 shows the dependence of TOF of carbon deposition and its selectivity on the dispersion of reduced Ni metal on the basis of Table 1. The number of surface Ni atoms can be estimated by the consumption of hydrogen at room temperature assuming $H/Ni_s = 1$. From Fig. 12, TOF and selectivity of carbon deposition were very dependent on the dispersion of reduced Ni metal. At lower dispersion, TOF and selectivity of carbon deposition were higher. This indicated that small nickel particles inhibit carbon

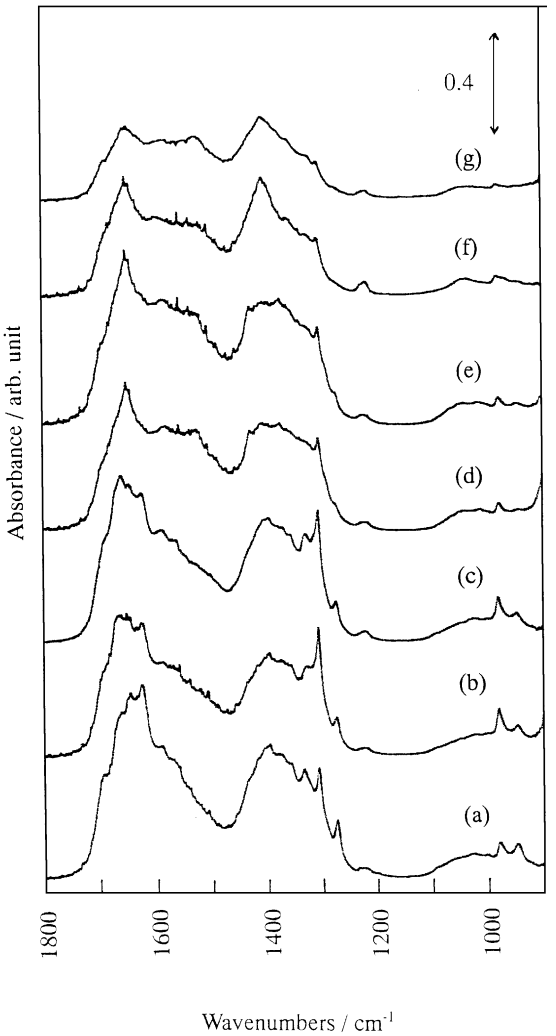

FIG. 10. FTIR spectra of CO_2 adsorption on catalysts. (a) MgO, (b) $Ni_{0.03}Mg_{0.97}O$, (c) $Ni_{0.05}Mg_{0.95}O$, (d) $Ni_{0.07}Mg_{0.93}O$, (e) $Ni_{0.15}Mg_{0.85}O$, (f) 1.0 mol% Ni/MgO, (g) 3.0 mol% Ni/MgO. Reduction pretreatment, H_2 reduction at 1123 K; FTIR measurement, room temperature, evacuation after CO_2 introduction at $P_{CO_2} = 1.3$ kPa, 2 cm^{-1} resolution.

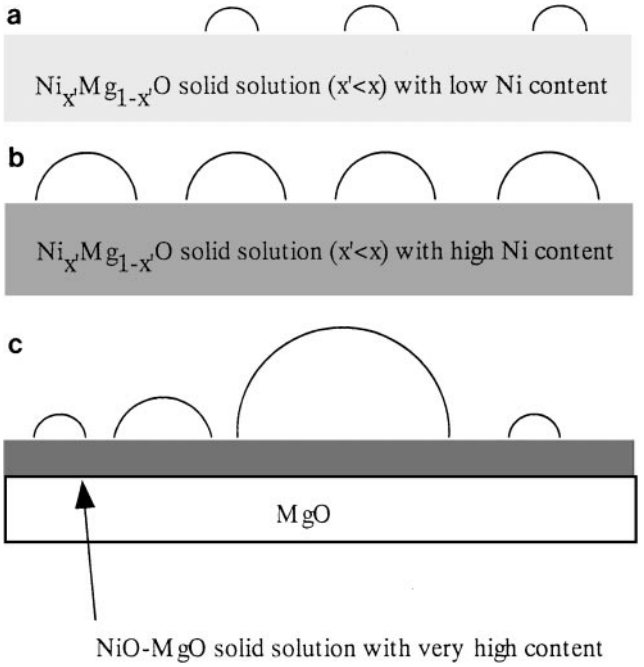

FIG. 11. Structural image of solid solution catalysts with low and high nickel content, supported catalysts, (a) nickel magnesia solid solution catalysts with low nickel content, (b) nickel magnesia solid solution catalysts with high nickel content, (c) supported Ni/MgO catalysts.

deposition in CO_2 reforming of methane. On the other hand, a clear dependence of TOF on CO formation on the dispersion of reduced Ni metal was not found. The structure sensitivity of this reaction has been discussed on Rh- and Ir-supported catalysts (12), and it has been shown that this reaction is classified as structure insensitve. But in our case, this reaction is structure sensitive.

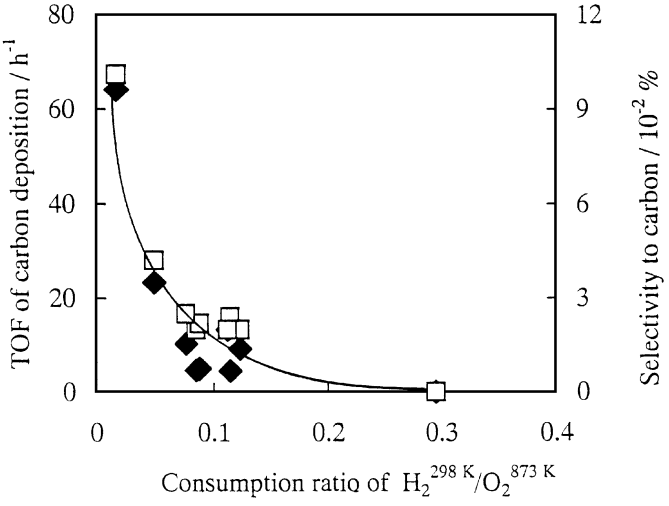

FIG. 12. Dependence of TOF (◆) on carbon formation and its selectivity (□) on the ratio of consumption $H_2^{298\ K}/O_2^{873\ K}$. TOF, selectivity, and ratio of consumption are based on Table 1.

It has been reported that the properties of support, especially basicity, are very important in CO_2 reforming of methane (57, 58). It was found that a large amount of carbon was deposited during CO_2 reforming of methane on $NiO–Al_2O_3$ catalysts with extremely small nickel particles (58). In addition, nickel particles interacting with support on 3 mol% Ni/MgO seemed to have high resistance to carbon deposition. In terms of support basicity, NiO–MgO solid solutions with low nickel content may be similar to MgO. It is suggested that a synergistic effect of high dispersion of nickel metal particle and basicity of support surface produces high resistance to carbon deposition in CO_2 reforming of methane. This can help the design of excellent catalysts for CO_2 reforming of methane.

CONCLUSION

(1) Reduced $Ni_xMg_{1-x}O$ ($x = 0.03–0.10$) solid solution catalysts showed higher resistance to carbon formation than Ni/MgO-supported catalysts.

(2) The increase in Ni content brought about a negative effect on the anticoking performance in CO_2 reforming of methane on reduced solid solution catalysts.

(3) Deposited carbon was formed on the larger Ni particles during the reforming reaction on 3 mol% Ni/MgO.

(4) A synergistic effect between high Ni dispersion and basicity of support surface is suggested to produce very high resistance to carbon formation in CO_2 reforming of methane on reduced $Ni_{0.03}Mg_{0.97}O$ solid solution catalysts.

ACKNOWLEDGMENTS

A part of this research was supported by the Future Program of Japan Society for the Promotion of Science under the Project "Synthesis of Ecological High Quality of Transportation Fuels" (JSPS-RFTF98P01001) and Proposal-Based New Industry Creative Type Technology R&D Promotion Program from the New Energy and Industrial Technology Development Organization (NEDO) of Japan.

REFERENCES

1. Gadalla, A. M., and Bower, B., *Chem. Eng. Sci.* **43**, 3049 (1988).
2. Gadalla, A. M., and Sommer, M. E., *Chem. Eng. Sci.* **44**, 2825 (1989).
3. Gadalla, A. M., and Sommer, M. E., *J. Am. Ceram. Soc.* **72**, 683 (1989).
4. Rostrup-Nielsen, J. R., and Hansen, J.-H. B., *J. Catal.* **144**, 38 (1993).
5. Erdohelyi, A., Cserenyi, J., and Solymosi, F., *J. Catal.* **141**, 287 (1993).
6. Tokunaga, O., Osada, Y., and Ogasawara, S., *Fuel* **68**, 990 (1989).
7. Richardson, J. T., and Paripatyadar, S. A., *Appl. Catal.* **61**, 293 (1990).
8. Chubb, T. A., *Sol. Energy* **24**, 341 (1980).
9. McCrary, J., McCrary, G. E., Chubb, T. A., Nemecek, J. J., and Simmons, D. E., *Sol. Energy* **29**, 141 (1982).
10. Fish, J. D., and Hawn, D. C., *J. Sol. Energy Eng.* **109**, 215 (1987).
11. Perera, J. S. H. Q., Couves, J. W., Sankar, G., and Thomas, J. M., *Catal. Lett.* **11**, 219 (1991).
12. Mark, M. F., and Maier, W. F., *J. Catal.* **164**, 122 (1996).
13. Kroll, V. C. H., Swaan, H. M., and Mirodatos, C., *J. Catal.* **161**, 409 (1996).
14. Kim, G. J., Cho, D. S., Kim, K. H., and Kim, J. H., *Catal. Lett.* **28**, 41 (1994).

15. Ashcroft, A. T., Cheetham, A. K., Green, M. L. H., and Vernon, P. D. F., *Nature* **352**, 225 (1991).
16. Takayasu, O., Hirose, E., Matsuda, N., and Matsuura, I., *Chem. Express* **6**, 447 (1991).
17. Blom, R., Dahl, I. M., Slagtern, A., Sortland, B., Spjelkavik, A., and Tangstad, E., *Catal. Today* **21**, 535 (1994).
18. Rostrup-Nielsen, J. R., *Stud. Surf. Sci. Catal.* **81**, 25 (1994).
19. Solymosi, F., Kutsain, G., and Erdohelyi, A., *Catal. Lett.* **11**, 149 (1991).
20. Osaki, T., Horiuchi, T., Suzuki, K., and Mori, K., *Catal. Lett.* **35**, 39 (1995).
21. Zhang, Z., and Verykios, X. E., *J. Chem. Soc. Chem. Commun.*, 71 (1995).
22. Zhang, Z., and Verykios, X. E., *Appl. Catal. A* **138**, 109 (1996).
23. Zhang, Z., Verykios, X. E., MacDonald, S. M., and Affrossman, S., *J. Phys. Chem.* **100**, 744 (1996).
24. Chen, Y.-G., and Ren, J., *Catal. Lett.* **29**, 39 (1994).
25. Fujimoto, K., Omata, K., Nozaki, T., Yamazaki, O., and Han, Y., *Energy Convers. Mgmt.* **3**, 529 (1992).
26. Yamazaki, O., Nozaki, T., Omata, K., and Fujimoto, K., *Chem. Lett.*, 1953 (1992).
27. Yamazaki, O., Tomishige, K., and Fujimoto, K., *Appl. Catal. A* **13**, 649 (1996).
28. Chen, Y.-G., Yamazaki, O., Tomishige, K., and Fujimoto, K., *Catal. Lett.* **39**, 91 (1996).
29. Chen, Y.-G., Tomishige, K., and Fujimoto, K., *Appl. Catal. A* **161**, L11 (1997).
30. Chen, Y.-G., Tomishige, K., Yokoyama, K., and Fujimoto, K., *Appl. Catal. A* **165**, 335 (1997).
31. Tomishige, K., and Fujimoto, K., *Catal. Surv. Jpn.* **2**, 3 (1998).
32. Yamazaki, O., Doctoral Thesis, the University of Tokyo (1996).
33. Tomishige, K., Chen, Y.-G., Li, X., Yokoyama, K., Sone, Y., Yamazaki, O., and Fujimoto, K., *Stud. Surf. Sci. Catal.* **114**, 375 (1998).
34. Chen, Y.-G., Tomishige, K., and Fujimoto, K., *Chem. Lett.*, 999 (1997).
35. Tomishige, K., Chen, Y.-G., Yamazaki, O., Himeno, Y., Koganezawa, Y., and Fujimoto, K., *Stud. Surf. Sci. Catal.* **119**, 861 (1998).
36. Ruckenstein, E., and Hu, Y. H., *Appl. Catal. A*: **133**, 149 (1995).
37. Hu, Y. H., and Ruckenstein, E., *Catal. Lett.* **36**, 145 (1996).
38. Hu, Y. H., and Ruckenstein, E., *J. Catal.* **163**, 306 (1996).
39. Hu, Y. H., and Ruckenstein, E., *Langmuir* **13**, 2055 (1997).
40. Ruckenstein, E., and Hu, Y. H., *Appl. Catal. A* **154**, 185 (1997).
41. Bradford, M. C. J., and Vannice, M. A., *Appl. Catal. A* **142**, 97 (1996).
42. Swaan, H. M., Kroll, V. C. H., Martin, G. A., and Mirodatos, C., *Catal. Today* **21**, 571 (1994).
43. Kroll, V. C. H., Swaan, H. M., Lacombe, S., and Mirodatos, C., *J. Catal.* **164**, 387 (1997).
44. Trimm, D. L., *Catal. Rev. Sci. Eng.* **16**, 155 (1977).
45. Rostrup-Nielsen, J. R., *in* "Catalysis Science and Technology" (J. R. Anderson and M. Boudart, Eds.), Vol. 5. Springer-Verlag, New York, 1984.
46. Parmaliana, A., Arena, F., Frusteri, F., and Giordano, N., *J. Chem. Soc. Faraday Trans.* **86**, 2663 (1990).
47. Kale, G. M., *J. Am. Cerm. Soc.* **74**, 2209 (1991).
48. Baker, R. T. K., Harris, P. S., Thomas, R., and Waite, R., *J. Catal.* **30**, 86 (1973).
49. Bartholomew, C. H., Pannell, R. B., and Butler, J. L., *J. Catal.* **65**, 335 (1980).
50. Zecchina, A., Spoto, G., Coluccia, S., and Guglielminotti, E., *J. Chem. Soc. Faraday Trans.* **80**, 1875 (1984).
51. Zecchina, A., Spoto, G., Coluccia, S., and Guglielminotti, E., *J. Chem. Soc. Faraday Trans.* **80**, 1891 (1984).
52. Fukuda, Y., and Tanabe, K., *Bull. Chem. Soc. Jpn.* **46**, 1616 (1973).
53. Lercher, J. A., Colombier, C., and Noller, H., *J. Chem. Soc. Faraday Trans.* **80**, 949 (1984).
54. Philipp, R., and Fujimoto, K., *J. Phys. Chem.* **96**, 9035 (1992).
55. Gopal, P. G., Schneider, R. L., and Watters, K. L., *J. Catal.* **105**, 366 (1987).
56. Efstathiou, A. M., Kladi, A., Tsipouriari, V. A., and Verykios, X. E., *J. Catal.* **158**, 64 (1996)
57. Horiuchi, T., Sakuma, K., Fukui, T., Kubo, Y., Osaki, T., and Mori, T., *Appl. Catal. A* **144**, 111 (1996).
58. Chen, Y.-G., Tomishige, K., and Fujimoto, K., *J. Catal.* **181**, 91 (1999).